arXiv:1409.1355v2 [astro-ph.CO] 10 Oct 2014

KIAS-P14054

Breaking CMB degeneracy in dark energy through LSS

Seokcheon Lee
School of Physics, Korea Institute for Advanced Study, Heogiro 85, Seoul 130-722, Korea

The cosmic microwave background (CMB) and large scale structure (LSS) are complementary probes to investigate the early and late time universe. After the current accomplishment of the high accuracies of CMB measurements, accompanying precision cosmology from LSS data is emphasized. We investigate the dynamical dark energy (DE) models which can produce the same CMB angular power spectra as that of the ΛCDM model with less than a subpercent level accuracy. If one adopts the dynamical DE models using the so-called Chevallier-Polarski-Linder (CPL) parametrization, $\omega \equiv \omega_0 + \omega_a(1-a)$, then one obtains models $(\omega_0, \omega_a) = (-0.8, -0.767), (-0.9, -0.375), (-1.1, 0.355), (-1.2, 0.688)$ named as M8, M9, M11, and M12, respectively. The differences of the growth rate, f which is related to the redshift space distortions (RSD) between different DE models and the ΛCDM model are about 0.2 % only at z=0. The difference of f between M8 (M9, M11, M12) and the ΛCDM model becomes maximum at $z \simeq 0.25$ with -2.4 (-1.2, 1.2, 2.5) %. This is a scale-independent quantity. One can investigate the one-loop correction of the matter power spectrum of each model using the standard perturbation theory in order to probe the scale-dependent quantity in the quasi-linear regime (*i.e.* $k \leq 0.4\mathrm{h}^{-1}$ Mpc). The differences in the matter power spectra including the one-loop correction between M8 (M9, M11, M12) and the ΛCDM model for $k = 0.4\mathrm{h}^{-1}$ Mpc scale are 1.8 (0.9, 1.2, 3.0) % at $z = 0$, 3.0 (1.6, 1.9, 4.2) % at $z = 0.5$, and 3.2 (1.7, 2.0, 4.5) % at $z = 1.0$. The bigger departure from -1 of ω_0, the larger the difference in the power spectrum. Thus, one should use both the RSD and the quasi-linear observable in order to discriminate a viable DE model among a slew of models which are degenerated in CMB. Also we obtain the lower limit on $\omega_0 > -1.5$ from the CMB acoustic peaks and this will provide the useful limitation on phantom models.

PACS numbers: 95.36.+x, 98.65.-r, 98.80.-k

1. INTRODUCTION

Both the cosmic microwave background (CMB) and the large scale structure (LSS) in the Universe have been used to constrain cosmological parameters. Especially, the growth history of the matter fluctuation from LSS is used to reveal the properties of dark energy (DE). Although CMB anisotropies furnish the limited information about the DE on their own, CMB constraints on the geometry and the matter (radiation) content of the Universe play a crucial role in probing DE when combined with low redshift surveys. CMB data supply measurements of the observed angular size of the sound horizon at recombination $\theta_s = r_s/d_A^{(c)}$ from the angular location of the acoustic peaks to better than 0.1 % precision at 1 σ [1]. Even though the sound horizon at the time of last scattering, $r_s(z_*)$, is insensitive to the properties of DE, the comoving angular diameter distance at which we are observing the fluctuations, $d_A^{(c)}(z_*)$, does depend on the properties of DE.

CMB also provides the best way of fixing the amplitude of cosmological fluctuations on the largest scales [2, 3]. In addition to this, as a secondary anisotropies the different amounts of potentials decay caused by different DE models lead to the net energy change of photons called the Integrated Sachs-Wolfe (ISW) effect. The alternative normalization is σ_8, the *rms* linear matter fluctuation in spheres of radius 8 h^{-1} Mpc inferred from abundances of clusters. However, this scale is not sufficiently large to remove the non-linear effect and fluctuations at these scales are still well inside the horizon to depend on its evolution.

Redshift space distortions (RSD) are the consequence of peculiar motions on the measurement of the power spectrum from a galaxy redshift survey. On large scales, coherent bulk flows bound to a over density out of voids are coherent towards the central mass which lead to an enhancement in the density inferred in the redshift space. The enhancement of the power spectrum due to RSD, under the linear perturbation theory assumption with the plane parallel approximation is given by $P_s(k,\mu) = (1+\beta\mu^2)^2 P_r(k,\mu)$. β is a

so-called the RSD parameter defined as $\beta = f/b$ where $f = d\ln\delta/d\ln a$ is the growth rate and b is the bias factor [4].

Our main interest is to understand the dark-energy effect on the matter power spectrum in a quasi-linear regime. Analytical solutions are presented for the dynamical DE model parameterized so-called Chevallier-Polarski-Linder (CPL) parametrization, $\omega \equiv \omega_0 + \omega_a(1-a)$ [5]. Each dynamical model can produce the same CMB power spectrum as those of ΛCDM model by obtaining the proper ω_0 and ω_a fixing all other cosmological parameters. Similar approach for the numerical simulation has been investigated [6] and the approximate approach using the standard perturbation theory (SPT) for the one-loop correction matter power spectrum has also been studied [7].

In the next section, we obtain the proper values of (ω_0, ω_a) to produce the same angular size of the sound horizon power as that of ΛCDM model. We compare the CMB power spectra of models. In section 3, we compare the predicted values of RSD for corresponding models. In section 4, we obtain the one-loop matter power spectrum of each model using SPT and compare it with that of ΛCDM model. We conclude in the last section. In the appendix, we extend the models including ones will be possibly ruled out in future survey.

2. DARK ENERGY AND COSMIC MICROWAVE BACKGROUND

The CMB is a power window to probe the early universe. At the last scattering surface, z_* where the photons interact with matter for the last time, it shows tiny temperature fluctuations that correspond to slightly different densities, representing the seeds of LSS. The pressure of the photons tends to erase temperature anisotropies, whereas the gravitational attraction of the baryons makes them tend to collapse. These two effects compete to create acoustic oscillations with CMB peak structure. One calls the characteristic angular size of the fluctuation in the CMB as the acoustic scale. It is determined by the sound horizon at the last scattering, $r_s(z_*)$ and the comoving angular diameter distance, $d_A^{(c)}(z_*)$. We adopt CPL parametrization of DE equation of state, ω. The acoustic angular size is defined by

$$\theta_s(z_*) = \frac{r_s(z_*)}{d_A^{(c)}(z_*)}\,, \tag{2-1}$$

where

$$r_s(z_*) = \int_0^{t_*}\frac{c_s dt}{a} = \frac{c}{\sqrt{3}H_0}\int_{z_*}^{\infty}\frac{dz'}{\sqrt{1+R(z')}E(z')}\,, \text{where } R \equiv \frac{3\rho_b}{4\rho_\gamma}\,, \tag{2-2}$$

$$d_A^{(c)}(z_*) \equiv (1+z)d_A(z_*) = \frac{c}{H_0}\int_0^{z_*}\frac{dz'}{E(z')}\,, \tag{2-3}$$

$$E(z) \equiv \frac{H}{H_0} \tag{2-4}$$

$$= \sqrt{\Omega_{\rm m0}(1+z)^3 + \frac{\Omega_{\rm m0}}{1+z_{\rm eq}}(1+z)^4 + (1-\Omega_{\rm m0}\frac{2+z_{\rm eq}}{1+z_{\rm eq}})(1+z)^{3(1+w_0+w_a)}\exp[-3w_a(\frac{z}{1+z})]}\,.$$

where H_0 is the present value of the Hubble parameter, $\Omega_{\rm m0}$ is the present value of the matter energy density contrast, and $z_{\rm eq}$ is the matter and the radiation equality epoch. $\theta_s(z_*)$ is measured by the positions of the peaks but not by their amplitudes and this it is quite robust. Also, $\theta_s(z_*)$ is tightly constrained from the observation, it can be safely used to constrain the cosmological parameters. From Eqs. (2-1)-(2-4), one can find that $d_A^{(c)}(z_*)$ depends on ω and so does $\theta_s(z_*)$. If one keeps all other cosmological parameters fixed except ω, then one is able to obtain the viable values of (ω_0, ω_a) which can produce the same $\theta_s(z_*)$ as that of ΛCDM model. We find the viable models and show their (ω_0, ω_a) values in Table. I.

Models	(ω_0, ω_a)	σ_8	t_0 (Gyr)
M8	(-0.8,-0.767)	0.850	13.40
M9	(-0.9,-0.375)	0.848	13.43
ΛCDM	(-1.0,0.0)	0.845	13.46
M11	(-1.1,0.355)	0.842	13.50
M12	(-1.2,0.688)	0.837	13.54

TABLE I: σ_8 and the age of the Universe in (Gyr), t_0 for CMB degenerated DE models.

We put $\Omega_{\rm m0} = 0.3$, $\Omega_{\rm b0} = 0.0462$, $\Omega_{\gamma 0} = 5.04\times10^{-5}$, $H_0 = 70$h km/sec/Mpc, $z_{\rm eq} = 3513$, and $z_* = 1089.73$. This set of parameters produces $\theta_s(z_*) = 0.0105$ for the ΛCDM. If we vary the value of ω_0 from -1.2 to -0.8 to obtain the same value of $\theta_s(z_*)$ as ΛCDM, then we obtain ω_a values as given in the Table. I. We label each model (ω_0, ω_a) = (-0.8,-0.767), (-0.9,-0.375), (-1.1,0.355), and (-1.2,0.688) as M8, M9, M11, and M12, respectively.

We show the CMB angular power spectrum of each model and its difference from ΛCDM model one in Fig. 1. As we expect, the CMB angular power spectra between models are almost same to one another as shown in the left panel of the Fig. 1. Dashed, dotdashed, solid, dotted, and long-dashed lines correspond (ω_0, ω_a) = (-0.8,-0.767), (-0.9,-0.375), (-1.0, 0), (-1.1,0.355), and (-1.2,0.688), respectively. If we investigate the differences of CMB power spectra between DE models and ΛCDM model, then they are less than 1 % for all model when $l \geq 5$. The difference in the large scale is due to the integrated Sachs Wolfe (ISW) effect caused by gravitational redshift occurring between the surface of last scattering and the present epoch. The different DE models produce the different large-scale gravitational potential energy wells and hills evolution and they cause changing the energy of photons passing through them. This is shown in the right panel of Fig. 1. Dashed, dotdashed, dotted, and long dashed lines correspond the angular power spectra differences between ΛCDM and (ω_0, ω_a) = (-0.8,-0.767), (-0.9,-0.375), (-1.1,0.355), and (-1.2,0.688), respectively. Observationally it is impossible to distinguish the CMB angular power spectra for these different models at large scale due to the cosmic variance.

CMB with the different DE models also provides the different normalization at large scale as [8, 9]

$$P(k,a) = Ak^{n_s}T(k)^2\Big(\frac{D(a)}{D_0}\Big)^2 \equiv 2\pi^2\delta_H^2\Big(\frac{c}{H_0}\Big)^{n_s+3}k^{n_s}T(k)^2\Big(\frac{D(a)}{D_0}\Big)^2, \tag{2-5}$$

where A is the normalization, n_s is the spectral index of the primordial adiabatic density perturbations, T is the transfer function, $D(a)(D_0)$ is the linear growth factor at $a(a = 1)$, and δ_H is the horizon crossing amplitude. From CMB observation, one can extract δ_H for the different DE models. In other word, δ_H can be a function of ω. However, theoretically this value is determined from the specific inflation model and thus we use the same value of δ_H (*i.e.* A) for the matter power spectrum analysis in Sec. 4. This also explains why we obtain the slightly different values of σ_8 for the different models.

$$\sigma_b^2(a) \equiv \Big\langle\Big|\frac{\delta M}{M(R,a)}\Big|^2\Big\rangle = \frac{1}{2\pi^2}\int_0^\infty k^2P(k,a)\Big|W(kR)\Big|^2_{R=8{\rm h}^{-1}\,{\rm Mpc}}dk\,. \tag{2-6}$$

Even though we use the same values of δ_H and n_s for the different DE models, one obtains the different $T(k)$s and these cause the slight different values of σ_8 as shown is table I.

3. DARK ENERGY AND REDSHIFT SPACE DISTORTIONS

Although Hubble's law determines the redshift corresponds to true distance, peculiar velocities not associated with the Hubble flow cause distortions in redshift space. These peculiar motions produce two different types of distortion to the matter power spectrum. On small scales, random velocity dispersions in galaxy clusters cause structure to appear elongated with long thin filaments in redshift space point directly back at observer. This is called as "the finger of God" effect. On large scales, peculiar velocities of galaxies bound to a central mass during their infall. Peculiar velocities are coherent towards the central mass and

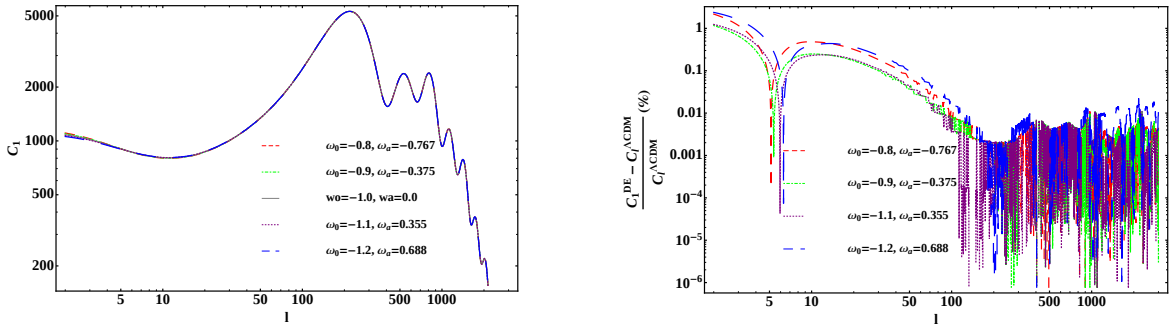

FIG. 1: CMB angular power spectra and their differences. left) CMB angular power spectra for M8 (dashed), M9 (dot-dashed), ΛCDM (solid), M11 (dotted), and M12 (long-dashed), respectively. right) Differences between CMB angular power spectrum of ΛCDM model and that of M8 (dashed), M9 (dot-dashed), M11 (dotted), and M12 (long-dashed), respectively.

cause the deviation of measured redshifts from a pure Hubble's law. This leads to an enhancement in the density inferred in redshift space and called as Redshift space distortions (RSD). The enhancement of the power spectrum due to RSD, under the linear perturbation theory assumption with the plane parallel approximation is given by $P_s(k,\mu) = (1+\beta\mu^2)^2 P_r(k,\mu)$ where P_s is the matter power spectrum in the redshift-space, P_r is one in the real space, $\mu = \hat{k}\cdot\hat{r}$ with $\hat{r}$ denoting the unit vector along the line of sight, and β is so-called the RSD parameter defined as $\beta = f/b$ where $f = d\ln\delta/d\ln a$ is the growth rate and b is the bias factor. Since one cannot directly measure the matter power spectrum, one has to investigate the RSD to the matter power spectrum of the galaxies as matter tracer in the galaxy redshift survey. Alternatively, one can use bias free RSD measurement using $f\sigma_8$.

In sub-horizon scales, one can define both the scale independent matter fluctuation $\delta(k,a) = D(a)\delta(k)$ and its growth rate $f = d\ln D/d\ln a$ where D is obtained from the linear perturbation theory

$$\frac{d^2D}{da^2} + \frac{3}{2a}\Big(1 - w\Omega_{de}\Big)\frac{dD}{da} - \frac{3}{2a^2}\Omega_m D = 0\,, \tag{3-1}$$

where $\Omega_m = 1-\Omega_{de} = \Big(1+(\Omega_{\rm m0}^{-1}-1)(1+z)^{3(w_0+w_a)}\exp[-3w_a(\frac{z}{1+z})]\Big)^{-1}$. D is the sub-horizon scale growth factor. Due to the ω dependence on $\Omega_{\rm m}(z)$, both D and f also depends on ω. However, the differences of D and f between different models are expected to be very small due to the similar background evolutions between them. We show this in Fig. 2.

If we compare the evolutions of the matter energy density contrast, $\Omega_{\rm m}(z)$ for different models, then M8 has the biggest $\Omega_{\rm m}(z)$ during the cosmic evolution. On the other hand, M12 maintains the smallest $\Omega_{\rm m}(z)$ among models. $\Omega_{\rm m}(z)$ provides the source term in Eq. (3-1). Thus, one can expect the biggest D for M8 and the smallest one for M12. This is shown in the left panel of 2. The difference of D between M8 (M9, M11, M12) and ΛCDM is depicted as dashed (dot-dashed, dotted, long-dashed) lines. At the present epoch, $z = 0$, the difference of D between M8 (M9, M11, M12) and ΛCDM is 0.4 (0.25, -0.2, -0.9) %. Thus, it is impossible to distinguish the different DE models with RSD when the measurement accuracy is bigger sub percent level. The difference of D becomes maximum at $z \simeq 0.8$ and it is about 1.2 (0.6, -0.7, -1.8) % for M8 (M9, M11, M12). We also show the differences of f between models in the right panel of Fig. 2. At present epoch, the differences between all models are less 0.2 %. The difference of f between M8 (M9, M11, M12) and ΛCDM becomes maximum around $z \simeq 0.25$ with -2.4 (-1.2, 1.2, 2.5) % deviation. Thus, measurements of f at specific epochs are quite important to probe the DE from RSD.

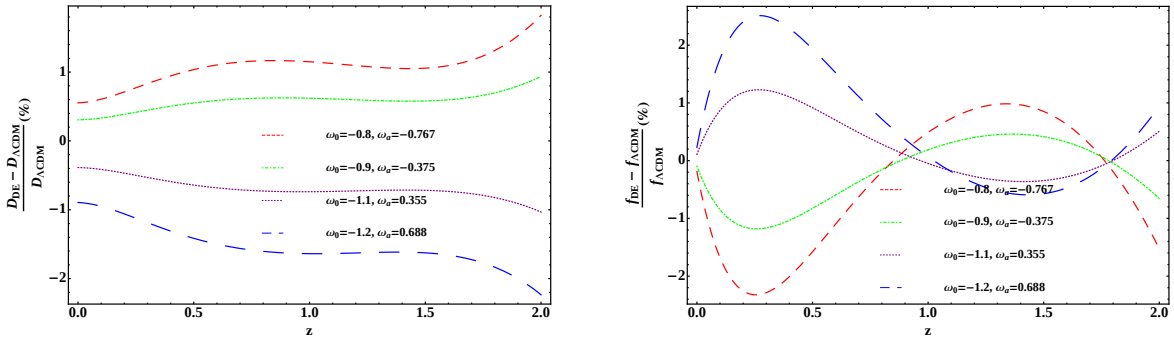

FIG. 2: Differences in the growth factor D and the growth rate f as a function of z left) Differences of growth factors Ds between DE models and the ΛCDM. The notation is M8 (dashed), M9 (dot-dashed), M11 (dotted), and M12 (long-dashed), respectively. right) Differences of growth rates fs between DE models and the ΛCDM. We use the same notation as a).

4. DARK ENERGY AND ONE-LOOP MATTER POWER SPECTRUM

The standard perturbation theory (SPT) has been widely used to investigate the correction to the linear power spectrum in a quasi-nonlinear regime. The exact solutions for the Fourier components of the matter density fluctuation $\hat{\delta}(\tau,\vec{k})$ and the divergence of the peculiar velocity $\hat{\theta}(\tau,\vec{k})$ has been obtained for general DE models up to third order [10]. One can investigate the DE effects on the matter power spectrum including the one-loop correction with these exact solutions.

The equations of motion of $\hat{\delta}(\tau,\vec{k})$ and $\hat{\theta}(\tau,\vec{k})$ in the Fourier space are given by

$$\frac{\partial\hat{\delta}}{\partial\tau}+\hat{\theta} = -\int d^3k_1\int d^3k_2\delta_{\rm D}(\vec{k}_{12}-\vec{k})\alpha(\vec{k}_1,\vec{k}_2)\hat{\theta}(\tau,\vec{k}_1)\hat{\delta}(\tau,\vec{k}_2)\,, \tag{4-1}$$

$$\frac{\partial\hat{\theta}}{\partial\tau}+\mathcal{H}\hat{\theta}+\frac{3}{2}\Omega_{\rm m}\mathcal{H}^2\hat{\delta} = -\frac{1}{2}\int d^3k_1\int d^3k_2\delta_{\rm D}(\vec{k}_{12}-\vec{k})\beta(\vec{k}_1,\vec{k}_2)\hat{\theta}(\tau,\vec{k}_1)\hat{\theta}(\tau,\vec{k}_2)\,, \tag{4-2}$$

where τ is the conformal time, $\vec{k}_{12}\equiv\vec{k}_1+\vec{k}_2$, $\delta_{\rm D}$ is the Dirac delta function, $\mathcal{H}\equiv\frac{1}{a}\frac{\partial a}{\partial\tau}$, $\Omega_{\rm m}$ is the matter energy density contrast, $\alpha(\vec{k}_1,\vec{k}_2)\equiv\frac{\vec{k}_{12}\cdot\vec{k}_1}{k_1^2}$, and $\beta(\vec{k}_1,\vec{k}_2)\equiv\frac{k_{12}^2(\vec{k}_1\cdot\vec{k}_2)}{k_1^2k_2^2}$.

Due to the mode coupling of the nonlinear terms shown in the right hand side of Eqs. (4-1) - (4-2), one needs to make a perturbative expansion in $\hat{\delta}$ and $\hat{\theta}$ [11]. One can introduce the proper perturbative series of solutions for the fastest growing mode D_n

$$\hat{\delta}(a,\vec{k}) \equiv \sum_{n=1}^{\infty}\hat{\delta}^{(n)}(a,\vec{k})\,, \tag{4-3}$$

$$\hat{\theta}(a,\vec{k}) \equiv \sum_{n=1}^{\infty}\hat{\theta}^{(n)}(a,\vec{k})\,, \tag{4-4}$$

where one can define the each order solution as

$$\hat{\delta}^{(1)}(a,\vec{k}) \equiv D_1(a)\delta_1(\vec{k})\,, \tag{4-5}$$

$$\hat{\theta}^{(1)}(a,\vec{k}) \equiv D_{\theta 1}(a)\theta_1(\vec{k}) \equiv -a\mathcal{H}\frac{dD_1}{da}\delta_1(\vec{k})\,, \tag{4-6}$$

$$\begin{aligned}\hat{\delta}^{(2)}(a,\vec{k}) &\equiv D_{21}(a)K_{21}(\vec{k}) + D_{22}(a)K_{22}(\vec{k}) \equiv D_1^2\Big[c_{21}(a)K_{21}(\vec{k}) + c_{22}(a)K_{22}(\vec{k})\Big] \equiv D_1^2(a)\delta_2(a,\vec{k}) \\ &\equiv D_1^2\int d^3k_1\int d^3k_2\delta_{\rm D}(\vec{k}_{12}-\vec{k})F_2^{(s)}(a,\vec{k}_1,\vec{k}_2)\delta_1(\vec{k}_1)\delta_1(\vec{k}_2)\,,\end{aligned} \tag{4-7}$$

$$\begin{aligned}\hat{\theta}^{(2)}(a,\vec{k}) &\equiv D_{\theta 21}(a)K_{21}(\vec{k}) + D_{\theta 22}(a)K_{22}(\vec{k}) \equiv D_1\frac{\partial D_1}{\partial\tau}\Big[c_{\theta 21}(a)K_{21}(\vec{k}) + c_{\theta 22}(a)K_{22}(\vec{k})\Big] \\ &\equiv D_1\frac{\partial D_1}{\partial\tau}\theta_2(a,\vec{k}) \equiv -D_1\frac{\partial D_1}{\partial\tau}\int d^3k_1\int d^3k_2\delta_{\rm D}(\vec{k}_{12}-\vec{k})G_2^{(s)}(a,\vec{k}_1,\vec{k}_2)\delta_1(\vec{k}_1)\delta_1(\vec{k}_2)\,,\end{aligned} \tag{4-8}$$

$$\begin{aligned}\hat{\delta}^{(3)}(a,\vec{k}) &\equiv D_{31}(a)K_{31}(\vec{k}) + \cdots + D_{36}(a)K_{36}(\vec{k}) \equiv D_1^3(a)\Big[c_{31}(a)K_{31}(\vec{k}) + \cdots + c_{36}(a)K_{36}(\vec{k})\Big] \\ &\equiv D_1^3(a)\int d^3k_1d^3k_2d^3k_3\delta_{\rm D}(\vec{k}_{123}-\vec{k})F_3^{(s)}(a,\vec{k}_1,\vec{k}_2,\vec{k}_3)\delta_1(\vec{k}_1)\delta_1(\vec{k}_2)\delta_1(\vec{k}_3)\,,\end{aligned} \tag{4-9}$$

where

$$c_{2i} = \frac{D_{2i}}{D_1^2}\,,\quad c_{\theta 2i} = \frac{D_{\theta 2i}}{D_1}\Big(\frac{\partial D_1}{\partial\tau}\Big)^{-1}\,,\quad c_{3i} = \frac{D_{3i}}{D_1^3}\,, \tag{4-10}$$

$$K_{21}(\vec{k}) = -\int d^3k_1\int d^3k_2\delta_{\rm D}(\vec{k}_{12}-\vec{k})\alpha(\vec{k}_1,\vec{k}_2)\theta_1(\vec{k}_1)\delta_1(\vec{k}_2)\,, \tag{4-11}$$

$$K_{22}(\vec{k}) = -\int d^3k_1\int d^3k_2\delta_{\rm D}(\vec{k}_{12}-\vec{k})\beta(\vec{k}_1,\vec{k}_2)\theta_1(\vec{k}_1)\theta_1(\vec{k}_2)\,, \tag{4-12}$$

$$\begin{aligned}F_2^{(s)}(a,\vec{k}_1,\vec{k}_2) &= \frac{1}{2}\Big[c_{21}\Big(\frac{\vec{k}_{12}\cdot\vec{k}_1}{k_1^2}+\frac{\vec{k}_{12}\cdot\vec{k}_2}{k_2^2}\Big) - 2c_{22}\frac{k_{12}^2(\vec{k}_1\cdot\vec{k}_2)}{k_1^2k_2^2}\Big] \\ &= c_{21} - 2c_{22}\left(\frac{\vec{k}_1\cdot\vec{k}_2}{k_1k_2}\right)^2 + \frac{1}{2}\Big(c_{21}-2c_{22}\Big)\vec{k}_1\cdot\vec{k}_2\left(\frac{1}{k_1^2}+\frac{1}{k_2^2}\right),\end{aligned} \tag{4-13}$$

$$\begin{aligned}G_2^{(s)}(a,\vec{k}_1,\vec{k}_2) &= \frac{1}{2}\Big[-c_{\theta 21}\Big(\frac{\vec{k}_{12}\cdot\vec{k}_1}{k_1^2}+\frac{\vec{k}_{12}\cdot\vec{k}_2}{k_2^2}\Big) + 2c_{\theta 22}\frac{k_{12}^2(\vec{k}_1\cdot\vec{k}_2)}{k_1^2k_2^2}\Big] \\ &= -c_{\theta 21} + 2c_{\theta 22}\left(\frac{\vec{k}_1\cdot\vec{k}_2}{k_1k_2}\right)^2 - \frac{1}{2}\Big(c_{\theta 21}-2c_{\theta 22}\Big)\vec{k}_1\cdot\vec{k}_2\left(\frac{1}{k_1^2}+\frac{1}{k_2^2}\right),\end{aligned} \tag{4-14}$$

$$F_3^{(s)}(a,\vec{k}_1,\vec{k}_2,\vec{k}_3) = \sum_{i=1}^{6}F_{3i}^{(s)}(a,\vec{k}_1,\vec{k}_2,\vec{k}_3)\,, \tag{4-15}$$

where explicit forms of $F_{3i}^{(s)}$ are given in the appendix of the reference [10]. Now we replace $D_1(a)$ as $D(a)$

Both the linear and the one-loop power spectra are defined as

$$P_1(a,k) = \left(\frac{D(a)}{D_0}\right)^2 P_{11}(k)\,, \tag{4-16}$$

$$P_2(a,k) = \left(\frac{D(a)}{D_0}\right)^4\Big[P_{22}(a,k) + 2P_{13}(a,k)\Big]\,, \tag{4-17}$$

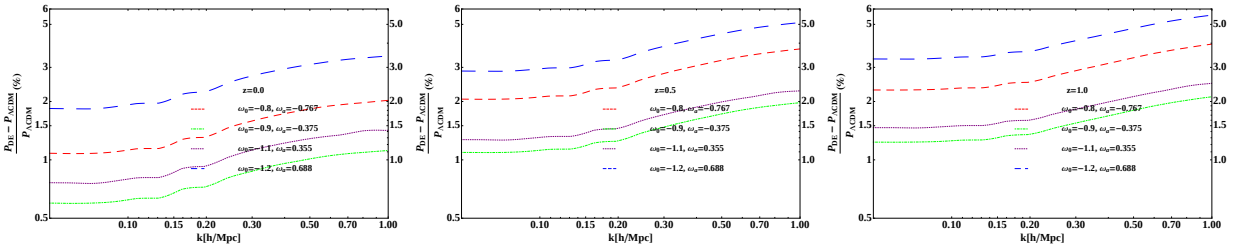

FIG. 3: The difference of matter power spectrum including one-loop correction between DE models and ΛCDM at different epoches. 1) Differences of matter power spectrum P between DE models and the ΛCDM at $z = 0$. The notation is M8 (dashed), M9 (dot-dashed), M11 (dotted), and M12 (long-dashed), respectively. 2) Differences of P at $z = 0.5$. 3) Difference of Ps at $z = 1.0$.

where $D_0 = D(a = 1)$, P_{22} and P_{13} are obtained as

$$P_{22}(a,k) = 2\int d^3q P_{11}(q)P_{11}(|\vec{k}-\vec{q}|)\Big[F_2^{(s)}(a,\vec{q},\vec{k}-\vec{q})\Big]^2 = \frac{(2\pi)^{-2}k^3}{2}\int_0^\infty dr P_{11}(kr)$$
$$\times \int_{-1}^{1} dx P_{11}\Big(k\sqrt{1+r^2-2rx}\Big)\left[\frac{(c_{21}+2c_{22})r+(c_{21}-2c_{22})x-2c_{21}rx^2}{(1+r^2-2rx)}\right]^2, \quad (4\text{-}18)$$

$$2P_{13}(a,k) = 6P_{11}(k)\int d^3q P_{11}(q)F_3^{(s)}(a,\vec{q},-\vec{q},\vec{k}) \quad (4\text{-}19)$$
$$= (2\pi)^{-2}k^3P_{11}(k)\int_0^\infty dr P_{11}(kr)\left[2c_{35}r^{-2}-\frac{1}{3}\Big(4c_{31}-8c_{32}+3c_{33}+24c_{35}-16c_{36}\Big)\right.$$
$$\left. -\frac{1}{3}\Big(4c_{31}-8c_{32}+12c_{33}-8c_{34}+6c_{35}\Big)r^2+c_{33}r^4+\Big(\frac{r^2-1}{r}\Big)^3\ln\Big|\frac{1+r}{1-r}\Big|\Big(c_{35}-\frac{1}{2}c_{33}r^2\Big)\right],$$

where $r = \frac{q}{k}$ and $x = \frac{\vec{q}\cdot\vec{k}}{qk}$. Terms with c_{2i} and c_{3i} represent the dark energy effect on the one-loop power spectrum.

We obtain the one-loop power spectra for different DE models by running the camb to obtain the linear power spectrum [12] using $n_s = 0.96$ and $A = 2.1 \times 10^{-9}$. The numerical integration range for q in Eqs. (4-18) and (4-19) is $10^{-6} \le q \le 10^2$. In this analysis, we use the normalization of A defined in Eq.(2-5) instead of σ_8. This is due to the fact that the specific inflation model predicts the specific value of A. However, σ_8 value is affected by the secondary effects like DE as shown in the table I.

Dark energy dependence on the one-loop matter power spectrum is depicted in Fig.3. We compare the matter power spectrum of each model with the one of ΛCDM. In the first column of Fig.3, we show the differences of P between models at the present epoch. The differences of P between M8 (M9, M11, M12) and ΛCDM are 1.1 (0.6, 0.8, 1.9) % for $k = 0.1\mathrm{h\,Mpc^{-1}}$ mode and 1.8 (0.9, 1.2, 3.0) % for $k = 0.4\mathrm{h\,Mpc^{-1}}$ one. In the second column of the figure, the differences of P between models at $z = 0.5$ are shown. The differences of P between M8 (M9, M11, M12) and ΛCDM are 2.1 (1.1, 1.3, 3.0) % for $k = 0.1\mathrm{h\,Mpc^{-1}}$ and 3.0 (1.6, 1.9, 4.2) % for $k = 0.4\mathrm{h\,Mpc^{-1}}$. The last column show the differences of P between models at $z = 1.0$. The differences of P between M8 (M9, M11, M12) and ΛCDM are 2.4 (1.2, 1.5, 3.4) % for $k = 0.1\mathrm{h\,Mpc^{-1}}$ and 3.3 (1.7, 2.0, 4.5) % for $k = 0.4\mathrm{h\,Mpc^{-1}}$.

We summarize the RSD and matter power spectra result in table II. We define $\Delta f = \frac{f_{\rm DE}-f_{\Lambda\rm CDM}}{f_{\Lambda\rm CDM}} \times 100(\%)$ and $\Delta P = \left|\frac{P_{\rm DE}-P_{\Lambda\rm CDM}}{P_{\Lambda\rm CDM}}\right| \times 100(\%)$. Both Δf and ΔP have the similar sensitivity on ω to separate DE models from ΛCDM at $z = 0.25$. However, ΔP can be used for almost entire epochs to distinguish DE

Models	Matter Power Spectrum ΔP (%)						RSD Δf (%)	
	z=0.0		z=0.5		z=1.0		z=0	z=0.25
	$k = 0.1$	0.4	0.1	0.4	0.1	0.4		
M8	1.1	1.8	2.1	3.0	2.4	3.2	0.2	-2.3
M9	0.6	0.9	1.1	1.6	1.2	1.7	0.2	-1.2
M11	0.8	1.2	1.3	1.9	1.5	2.0	0.2	1.2
M12	1.9	3.0	3.0	4.2	3.4	4.5	0.2	2.4

TABLE II: Summary of results in $\left|\frac{P_{\rm DE}-P_{\Lambda\rm CDM}}{P_{\Lambda\rm CDM}}\right|$ and $\frac{f_{\rm DE}-f_{\Lambda\rm CDM}}{f_{\Lambda\rm CDM}}$. k in unit of $\rm h\,Mpc^{-1}$.

models. As z increases, do does ΔP. This is not able to be achieved by RSD. Also the bigger the departure of ω_0 value from -1, the larger the ΔP.

5. CONCLUSIONS

Cosmic microwave background is degenerated for the different dark energy models even if one fix the other cosmological parameters. This degeneracy can be broken when one combine CMB with LSS. If we parameterize the dark energy equation of state by CPL, then we can find the various combination of (ω_0, ω_a) which can produce the same angular acoustic scale for each other. These models produce the different prediction for the growth rate which can be determined by the galaxy redshift space distortions. However, the growth rate is scale independent measurement and the differences between models can be reached the maxima at the specific epoch, like $z \simeq 0.25$. Even in this case, maximum difference is about 6 % for the considered models. If we consider the matter power spectrum including the one-loop correction, then the model dependence on the matter power spectrum is increased. If the accuracy of the future galaxy survey is reached to 5 %, then one can rule out many dark energy models which are degenerated by CMB and RSD.

Acknowledgments

This work were carried out using computing resources of KIAS Center for Advanced Computation. S.L would like to thank for the hospitality at APCTP during the program TRP.

APPENDIX

One can expand the CMB degenerated DE models. One is able to find the combinations of (ω_0, ω_a) to produce the same value of $\theta_s(z_*)$ for all models. If one just considers $\theta_s(z_*)$, then one can keep lowering the value of ω_0 to find the proper ω_a. We obtain corresponding ω_a values as given in the Table. III by varying ω_0. We label each model (ω_0, ω_a) = (-0.5,-2.035), (-0.6,-1.599), (-0.7,-1.176), (-0.8,-0.767), (-0.9,-0.375), (-1.1,0.355), (-1.2,0.688), (-1.3,0.993), (-1.4,1.266), and (-1.5,1.502) as M5, M6, M7, M8, M9, M11, M12, M13, M14, and M15, respectively.

However, CMB also provides the accurate measurements on its acoustic heights. From M5 to M14, the differences in the CMB angular power spectra between models are sub percent level for all scales. However, the differences of the CMB angular power spectrum between M15 and ΛCDM become more than 1 % for almost all scales. Thus, one can put the lower limit on ω_0 value (*i.e.* $\omega_0 > -1.5$). This can be used as a useful prior in other observation like SNe Ia. One might be able to rule out phantom models with $\omega_0 > 1.5$ if we use the same cosmological parameters as ΛCDM. M15 also produces about the 9 % deviation in σ_8

Model	(ω_0, ω_a)	σ_8	$\Delta\sigma_8$	Δf		$\Delta P(z=0.5)$ (%)	
				$z=0$	$z=0.25$	$k=0.1$	$k=0.4$
M5	(-0.5,-2.035)	0.855	1.183	-0.42	-5.56	4.85	6.59
M6	(-0.6,-1.599)	0.853	0.947	-0.35	-4.51	4.12	5.58
M7	(-0.7,-1.176)	0.852	0.828	-0.27	-3.43	3.28	4.44
M8	(-0.8,-0.767)	0.850	0.592	-0.19	-2.32	2.33	3.14
M9	(-0.9,-0.375)	0.848	0.355	-0.10	-1.18	1.25	1.69
M10	(-1.0,0)	0.845	0	0	0	0	0
M11	(-1.1,0.355)	0.842	-0.355	0.12	1.22	1.49	1.99
M12	(-1.2,0.688)	0.837	-0.947	0.23	2.50	3.37	4.48
M13	(-1.3,0.993)	0.830	-1.775	0.36	3.84	5.97	7.87
M14	(-1.4,1.266)	0.814	-3.669	0.52	5.26	10.51	13.71
M15	(-1.5,1.502)	0.770	-8.876	0.70	6.77	20.83	26.50

TABLE III: Summary of results in Δf and $|\Delta P|$ at z = 0.5. k in unit of $\mathrm{h\,Mpc^{-1}}$.

value from that of ΛCDM. If the accuracy of RSD observation at $z = 0.25$ reaches to 3 % level, then one can distinguish M5, M6, M7, M13, and M14 from ΛCDM.

If one further considers the matter power spectrum, then one can have the stronger constraint on ω_0. The difference of linear matter power spectra at the present epoch between M5 (M6, M7, M8, M9, M11, M12, M13, M14, M15) and ΛCDM becomes 2.2 (1.9, 1.5, 1.1, 0.6, 0.8, 1.9, 3.6, 7.3, 16.9) % at $k = 0.1\mathrm{h\,Mpc^{-1}}$. Thus, if the accuracy of the galaxy redshift survey reaches to 5 % level, then both M14 and M15 can be ruled out. If one considers the matter power spectrum including the one-loop correction, then one can have the even stronger constraints on ω. We consider the matter power spectrum including one-loop correcting using SPT at z = 1.0. The difference of the matter power spectra between M5 (M6, M7, M8, M9, M11, M12, M13, M14, M15) and ΛCDM becomes 4.85 (4.12, 3.28, 2.33, 1.25, 1.49, 3.37, 5.97, 10.51, 20.83) % at $k = 0.1\mathrm{h\,Mpc^{-1}}$. Also if we consider the scale $k = 0.4\mathrm{h\,Mpc^{-1}}$, then it becomes 6.59 (5.58, 4.44, 3.14, 1.69, 1.99, 4.48, 7.87, 13.71, 26.50) %. Thus, even M13 will be rule by the 5 % level accuracy measurement. These are summarized in table .III.

[1] P. A. R. Ade *et al.* (Planck Collaboration), Astron. & Astrophys. [arXiv:1303.5076].
[2] M. White and D. Scott, Comments on Astrophys.**18**, 289 (1996) [arXiv:astro-ph/9601170].
[3] E. F. Bunn and M. White, Astrophys. J. **480**, 6 (1997) [arXiv:astro-ph/9607060].
[4] N. Kaiser, Mon. Not. Roy. Astron. Soc. **227**, 1 (1987).
[5] M. Chevallier and D. Polarski, Int. J. Mod. Phys. D **10**, 213 (2001) [gr-qc/0009008]; E. V. Linder, Phys. Rev. Lett. **90**, 091301 (2003) [astro-ph/0208512].
[6] Matthew J. Francis, Geraint F. Lewis, Eric V. Linder, Mon. Not. Roy. Astron. Soc. **380**, 1079 (2007) [arXiv:0704.0312].
[7] R. Takahashi, Prog. Theor. Phys. **120**, 549 (2008) [arXiv:0806.1437].
[8] C.-P. Ma, R. R. Caldwell, P. Bode, and L. Wang, Astrophys. J. **521**, L1 (1999) [arXiv:astroph/ 9906174].
[9] S. Lee and K.-W. Ng, [arXiv:1010.2291].
[10] S. Lee, C. Park, and S. G. Biern, Phys. Lett. B **736**, 403 (2014) [arXiv:1407.7325].
[11] F. Bernardeau, S. Colombi, E. Gaztanaga, and R. Scoccimarro, Phys. Rept. **367**, 1 (2002) [arXiv:astro-ph/0112551].
[12] A. Lewis and A. Challinor, URL: http://www.camb.info